minerals

MDPI

Article

Sodium Lauroyl Glutamate as a Collector in Cassiterite Flotation

Zaihua Peng [1,2], Lei Sun [1,3], Yang Cao [1,3,*], Xiaohui Fan [1,3], Wei Sun [1,3] and Qingqing Wang [1,3]

[1] School of Minerals Processing and Bioengineering, Central South University, Changsha 410083, China
[2] Western Mining Yulong Copper Co., Ltd., Chengdu 854000, China
[3] Key Laboratory of Hunan Province for Clean and Efficient Utilization of Strategic Calcium-Containing Mineral Resources, Central South University, Changsha 410083, China
* Correspondence: caoyang@csu.edu.cn; Tel.: +86-0731-88830482

Abstract: In this paper, sodium lauroyl glutamate (SLG), a stable and inexpensive green surfactant, was used as a flotation collector for the first time in cassiterite flotation. The micro-flotation tests revealed that SLG could effectively collect cassiterite and have superior selectivity against quartz over a wide pH range, compared with benzohydroxamic acid (BHA). The maximum recovery of cassiterite in the presence of SLG was 93.2%, while the quartz recovery was consistently lower than 8%. The adsorption experiments and zeta potential measurements suggested SLG was chemisorbed onto the cassiterite surface. The Fourier transform infrared spectroscopy (FTIR) and X-ray photoelectron spectroscopy (XPS) analyses indicated that the polar groups of SLG anions (the carboxyl and amide groups) chelate with the Sn ions on the cassiterite surface to form five-membered rings. This structure made SLG attach firmly to the cassiterite surface, effectively recovering cassiterite. Lastly, a good flotation index was achieved in the bench-scale flotation tests using SLG as the collector, which confirmed its potential economic value in practical application.

Keywords: cassiterite; flotation; sodium lauroyl glutamate; five-membered rings

Citation: Peng, Z.; Sun, L.; Cao, Y.; Fan, X.; Sun, W.; Wang, Q. Sodium Lauroyl Glutamate as a Collector in Cassiterite Flotation. *Minerals* **2023**, *13*, 61. https://doi.org/10.3390/min13010061

Academic Editor: Hyunjung Kim

Received: 17 December 2022
Revised: 27 December 2022
Accepted: 29 December 2022
Published: 30 December 2022

1. Introduction

Cassiterite is an economically feasible tin mineral in the Earth's crust, with a tin content of 78.6% [1–4]. Gravity separation is the primary method for recovering cassiterite due to its high specific gravity [5–9]. However, as high-quality tin resources have been developed and utilized, cassiterite quality has gradually become poor, fine, and miscellaneous [10–12]. Gravity separation is no longer suitable for fine polymetallic cassiterite [13–15]. Instead, flotation has gradually been used in industry as flotation reagents advance [16–19].

Besides fatty acids, phosphonic acid, and dodecyl sulfate, various hydroxamic acid collectors were also utilized to float cassiterite [20,21]. Among these hydroxamic acid collectors, benzohydroxamic acid (BHA) has been extensively used as a collector for cassiterite flotation due to its easy availability and strong collecting ability [22–25]. Even so, some problems with BHA cannot be neglected, such as its large reagent consumption and poor acid/alkali resistance [26]. Previous studies found that metal ions can interact with tin-hydroxyl compounds to form metal-containing complexes on the cassiterite surface. Therefore, the active site on the cassiterite surface was changed from a single tin to tin species and metal-containing complexes, promoting cassiterite flotation [23,27]. Nevertheless, metal ions inevitably lead to environmental issues [28,29]. Therefore, discovering a viable substitute collector to achieve efficient activation is worthwhile.

Sodium lauroyl glutamate (SLG) is a sarcosine derivative surfactant composed of a non-polar hydrophobic hydrocarbon chain and a polar hydrophilic group containing a highly reactive carboxyl and amide-based amino acid, as shown in Figure 1. Due to the excellent metal chelating ability, foaming properties, low toxicity, low irritation, and good biodegradability of SLG [30–33], it is widely used in the petrochemical industry, and in biology, medicine, pharmacology, agriculture, and electroplating [34–36]. Therefore, this

study first used SLG as the collector on cassiterite flotation because of its special functional group, inexpensive, and environment-friendly characteristics.

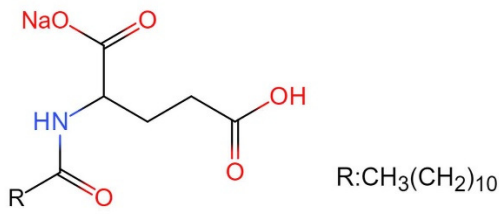

Figure 1. Molecule structure of sodium lauroyl glutamate.

Based on the micro-flotation tests, adsorption experiments, Zeta potential measurements, X-ray photoelectron spectroscopy (XPS), and Fourier transform infrared spectroscopy (FTIR), the flotation performance and adsorption mechanism of SLG on the cassiterite were revealed. A possible adsorption model of SLG on the cassiterite was inferred. Furthermore, the flotation effect of SLG on Xinzhai tin ore in Yunnan province is tested. This study gives new ideas for improving low-grade and complex cassiterite separation efficiency.

2. Materials and Methods

2.1. Materials and Reagents

Cassiterite and quartz samples used in this study were obtained from Yunnan Province, China. Their X-ray diffraction (XRD) and X-ray fluorescence (XRF) results are illustrated in Figure 2 and Tables 1 and 2, indicating that both of these minerals were of high purity. The massive mineral samples were crushed in a jaw crusher to −1 mm and ground with a porcelain mill to obtain the 38–74 μm and −10 μm size fractions separately. The fraction with a particle size of −74 + 38 μm was used in micro-flotation and adsorption experiments, while −10 μm size fractions were used for the zeta potential measurements, FTIR, and XPS analyses.

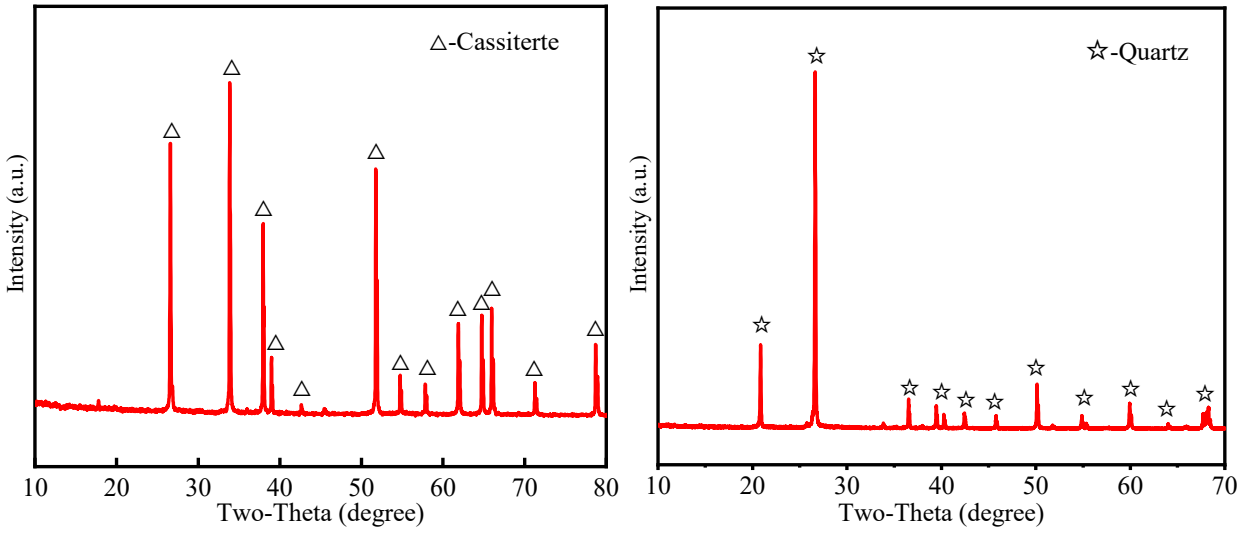

Figure 2. XRD of cassiterite and quartz samples.

Table 1. Chemical composition of cassiterite.

Component	SnO_2	Al_2O_3	MgO	CaO	TFe	Pb	SiO_2	Else
Content/%	97.98	0.22	0.35	0.24	0.18	0.17	0.35	0.51

Table 2. Chemical composition of quartz.

Component	SiO_2	Al_2O_3	MgO	CaO	K_2O	Na_2O	Fe_2O_3	Else
Content/%	98.68	0.41	0.08	0.13	0.21	0.06	0.21	0.22

All of the chemicals employed in this experiment were of analytical grade, except for those used in bench-scale flotation tests, which were of industrial grade. SLG and terpineol was selected as the collector and the frother, respectively. Solution pH values were regulated using a dilute hydrochloric acid solution and sodium hydroxide solution. Deionized water was used for micro-flotation, adsorption tests, zeta potential measurements, and XPS analyses. Tap water was used for bench-scale flotation tests.

2.2. Micro-Flotation Tests

The micro-flotation tests were performed in an XFGII flotation machine with a 40 mL plexiglass flotation cell. These tests were conducted in 5 stages (agitation 2 min, pH adjusted 2 min, various concentrations of collector addition 3 min, 3×10^{-5} mol/L frother addition 2 min, and flotation 4 min), as shown in Figure 3. After the flotation process, the concentrate and tailings were filtered, dried, and weighed to calculate the flotation recovery.

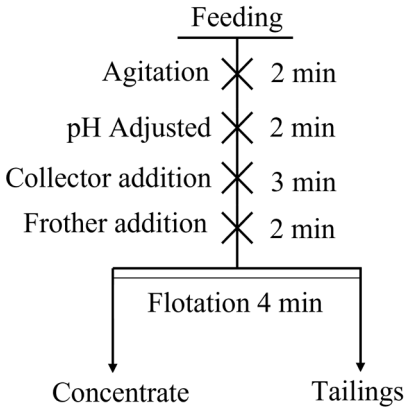

Figure 3. Flowsheet of the micro-flotation tests.

2.3. Adsorption Experiments

The amount of SLG adsorbed on the cassiterite surface was calculated using the residual content method. For sample preparation, 2 g of cassiterite samples were placed in a beaker with 35 mL DI water. After stirring for 4 min, the pulp pH was adjusted to the required value, followed by adding flotation reagents. The mixture was stirred for another 10 min. The resultant suspension was immediately subjected to solid–liquid separation using a TG16-WS centrifuge. The separated liquid was then collected to quantitatively analyze reagent concentration using an ultraviolet–visible spectrophotometer (UV-2700, Shimadzu, Japan). The adsorption amount of SLG on the cassiterite surface was calculated by Equation (1).

$$Q = \frac{(C_0 - C_1) \cdot V}{1000M \cdot S} \quad (1)$$

where Q is the adsorption amount (mol/g) of BHA on the cassiterite surface, C_0 is the initial BHA concentration (mol/L), C_1 is the residual BHA concentration in the pulp (mol/L), V is the volume of solution (L), M is the weight of cassiterite, and S is the specific surface area of the cassiterite sample, which is 0.4 $m^2 \cdot g^{-1}$.

2.4. Zeta Potential Measurements

The zeta potential of minerals was obtained using a Nano ZS90 Malvern Zetasizer (Malvern Panalytical, Malvern, UK) with 1×10^{-3} mol/L KCl background electrolyte solution. Before measurements, mineral samples were ground to -2 μm. For each test,

40 mg mineral was mixed with 40 mL KCl solution in the beaker for the desired duration with and without collectors. After adjusting the pulp pH, the dilute solution was stirred by a magnetic stirrer for 10 min and then settled for 5 min. The supernatant was taken for the zeta potential measurements. The tests for each condition were repeated 3 times and averaged.

2.5. XPS Analysis

A Thermo Scientific ESCALAB 250Xi photoelectron spectroscopy (Thermo Fisher Scientific, Waltham, MA, USA) using an Al Kα X-ray source operated at 200 W and 20 eV was conducted for the XPS analysis. The C1s spectrum at 284.8 eV was obtained and used as an internal standard to calibrate all measured spectra for charge compensation. An amount of 2.0 g of each mineral sample was pulverized to obtain a particle size of 5 µm in the agate mortar and then mixed with 100 mL of collector solution for 4 min. The solid fraction was filtered, washed with DI water, and vacuum dried in an oven at 50 °C before XPS analysis. All the XPS analyses were analyzed from three independent areas of the sample to check for the reproducibility of the results.

2.6. FTIR Analysis

The FTIR spectra of cassiterite were detected by RAffinity-1S FTIR (Shimadzu Instruments, Kyoto, Japan) within the wavenumber range of 500 cm^{-1}–4000 cm^{-1} at 25 °C. The samples used for the XPS analysis were also used for the FTIR analysis.

2.7. Bench-Scale Flotation Tests

The raw ore used in bench-scale flotation tests was obtained from the Xinzhai tin deposit in the southeastern part of Wenshan, Yunnan province, China. The massive raw ore was crushed into particles with sizes in the range of 1–2 cm and then ground to a particle size below 2 mm. The ground product was thoroughly mixed and homogenized to have a representative sample for chemical and particle size analyses, mineralogy characterization, and bench-scale flotation tests.

3. Results

3.1. Micro-Flotation Tests

Figure 4 depicts the recovery of cassiterite as a function of SLG and BHA concentrations. The flotation recovery of cassiterite increased sharply from 5.6% to 93.2% with the increase in SLG concentration and reached a plateau at 2×10^{-4} mol/L. However, only 38.6% of the cassiterite floated when 2×10^{-4} mol/L BHA was used. The optimum amount of SLG and BHA concentration that could be used in the cassiterite flotation has varied widely. Thus, the collecting performance of SLG was stronger than that of traditional collector BHA under the same conditions.

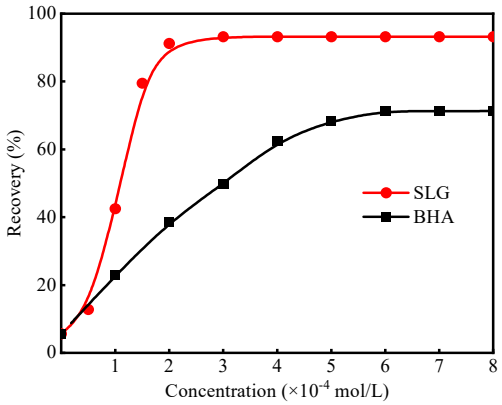

Figure 4. Flotation recovery of cassiterite as a function of SLG and BHA concentration.

The flotation recovery of cassiterite in the presence of SLG and BHA as a function of pulp pH was also investigated. As shown in Figure 5, the recovery of cassiterite first increased, then reached a plateau and decreased under a strong base solution using SLG or BHA as the collector. The recovery of cassiterite using SLG as a collector was over 50% in the whole pulp pH range. With regards to BHA, the floatability of cassiterite was very weak under high acid and alkaline environments. The maximum flotation recovery of cassiterite was floated by SLG and BHA, which were 93.1% and 71.05%, respectively, at pH 7.8–8.0. These results further indicated that SLG has good acid and alkali resistance.

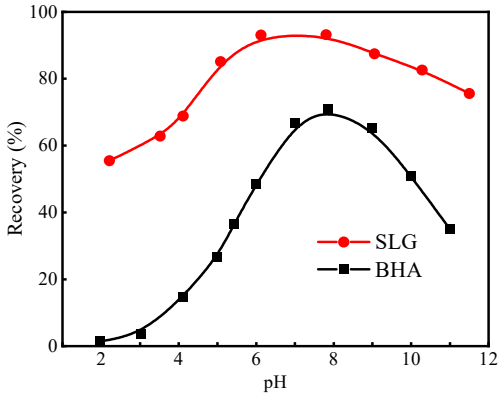

Figure 5. Flotation recovery of cassiterite using SLG or BHA as the collector as a function of pulp pH.

Furthermore, the artificial mixed mineral flotation tests were conducted to verify the selectivity of SLG at pH 7.8 ± 0.2, as shown in Figure 6. The mixed minerals were composed of cassiterite and quartz, and the mass ratio of cassiterite to quartz is 1:1. Figure 6 shows that cassiterite recovery increased sharply when SLG's initial concentration was less than 1.5×10^{-4} mol/L. When SLG was used as the collector, cassiterite displayed considerable floatability with a maximum recovery of over 93%. However, the quartz recovery has been consistently lower than 8%, and the recovery difference between cassiterite and quartz reached a maximum of 82.9%. SLG can be used to separate cassiterite and quartz effectively.

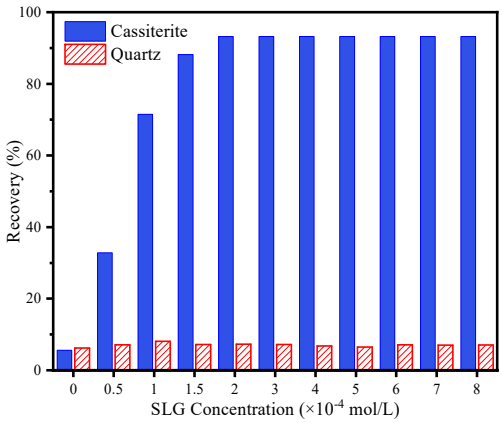

Figure 6. The flotation recovery of artificial mixed mineral (the mass ratio of cassiterite to quartz is 1:1) as a function of SLG concentration.

3.2. Adsorption Experiments

Figure 7 depicts the adsorption capacity of SLG and BHA on the cassiterite surface as a function of the SLG or BHA concentration at pH 7.8 ± 0.2. It could be seen that there is a gradual rise in the adsorption capacity of SLG and BHA on the cassiterite surface, with their concentration increasing until 3×10^{-4} mol/L and 6×10^{-4} mol/L, respectively. Above this range, their adsorption capacity remains stable. The adsorption capacity of BHA on the

cassiterite surface is always lower than in the presence of SLG, which is a similar result to that of the micro-flotation test. The maximum adsorption quantities of SLG and BHA were 43.6×10^{-6} mol/g and 32.9×10^{-6} mol/g when SLG and BHA concentrations reached 3×10^{-4} mol/L and 6×10^{-4} mol/L, respectively.

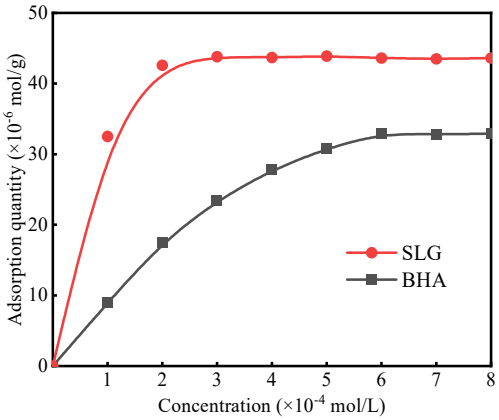

Figure 7. Adsorption capacity of SLG and BHA on cassiterite surface as a function of BHA and SLG concentration.

3.3. Zeta Potential Measurements

Zeta potential measurements reflect the state of charge on the mineral surface, which helps to reveal the adsorption process of the flotation reagents on the mineral surface. This section discusses the relationship between the zeta potential and pH of cassiterite surfaces floated using SLG as a collector.

Figure 8 reveals cassiterite has IEPs (iso-electric points) at about pH 4.01 in DI water, which is in accordance with previous research [37]. After SLG treatment, the IEP of cassiterite particles changed to pH 2.1, and its zeta potential was negatively shifted, inferring an increase in negative charges on the cassiterite surface. SLG mainly existed as an anionic species in aqueous solutions under pH > 2.5. As a result, after SLG adsorption, the zeta potentials of cassiterite particles became more negative. The results of zeta potential measurements speculated that chemical adsorption occurred on the cassiterite surface caused by SLG attachment.

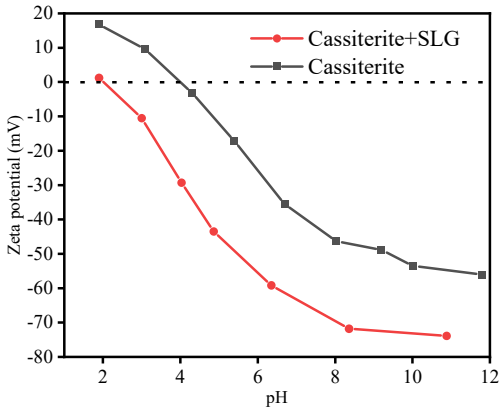

Figure 8. Zeta potential of cassiterite in the presence and absence of SLG.

3.4. XPS Analysis

X-ray photoelectron spectroscopy (XPS) studies were conducted mainly to determine the chemical state of metallic surface elements before and after a reaction. Figure 9 shows the XPS survey spectra of cassiterite before and after BHA or SLG treatment. The atomic concentration of elements on the cassiterite surface is shown in Table 3.

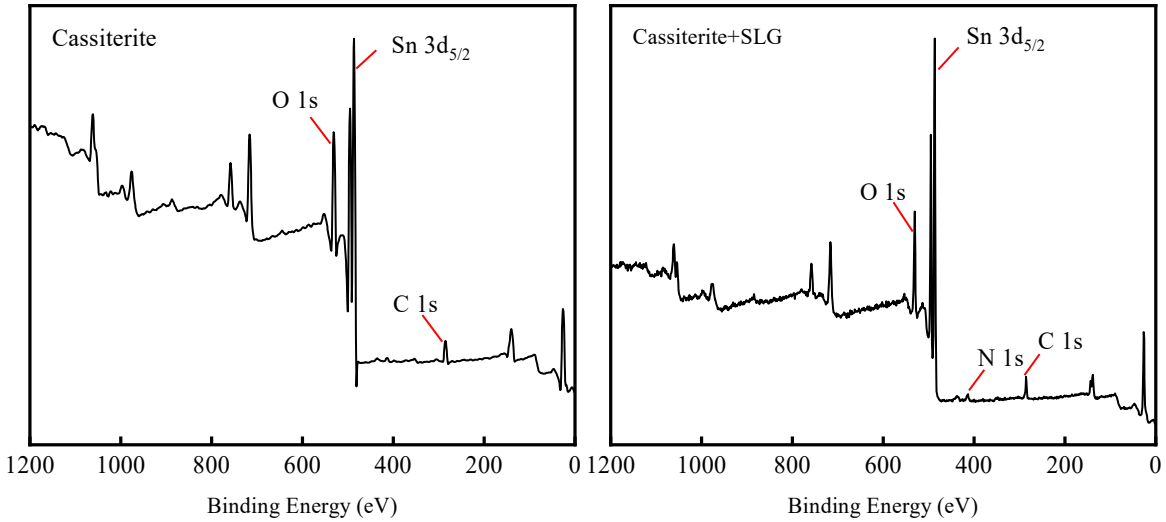

Figure 9. Survey scan XPS spectra of cassiterite sample in the presence and absence of SLG.

Table 3. Atomic concentrations of elements of cassiterite surface.

Element (Atomic %)	Cassiterite	Cassiterite + SLG	Δ
C	28.5	48.9	20.4
O	45.9	32.5	−13.4
Sn	25.6	17.4	−8.2
N	-	1.2	1.2

Δ is defined as the value of before treatment minus that of SLG treatment.

The results in Figure 9 revealed that a new N signal was displayed in the XPS survey spectra of cassiterite in the presence of SLG. It is also confirmed by an increasing atomic concentration of N in the cassiterite surface after SLG treatment, as shown in Table 3. These results indicated the coverage (adsorption) of cassiterite by SLG. To further examine the interaction of SLG with the cassiterite surface, the Sn 3d XPS spectra of the cassiterite before and after SLG treatment were detected (Figure 10).

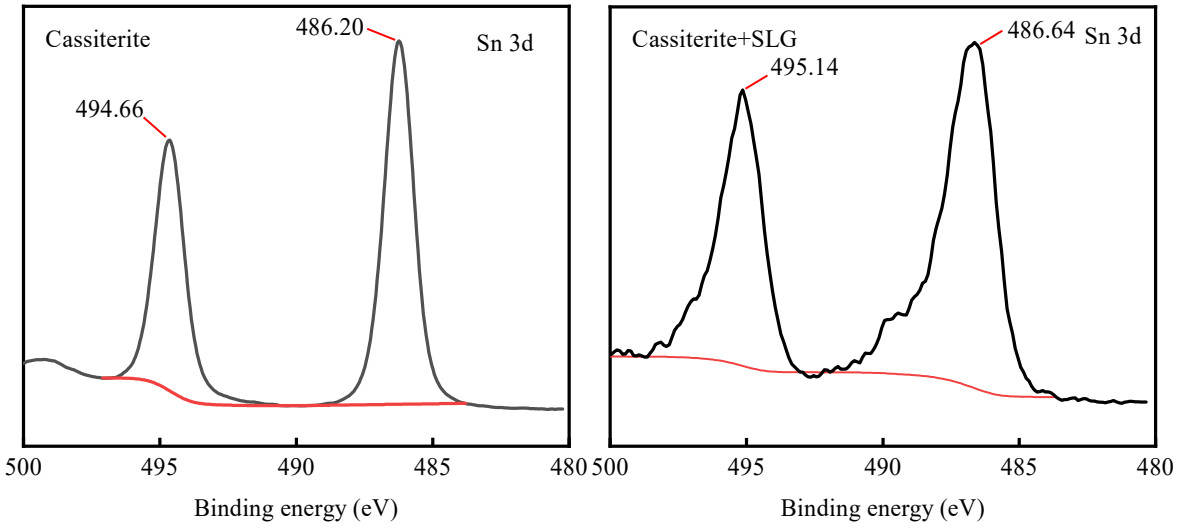

Figure 10. Sn 3d XPS analysis of cassiterite in the presence and absence of SLG.

As shown in Figure 10, the XPS bonds of Sn 3d for the original cassiterite had one double peak at 494.66 eV and 486.20 eV, which were assigned to Sn $3d_{3/2}$ and Sn $3d_{5/2}$, respectively. After SLG treatment, the Sn 3d peaks were shifted to the higher binding

energies of 495.14 eV and 486.64 eV, respectively. These features revealed that the chemical circumstances of the Sn atoms on the cassiterite surface had changed, indicating that SLG chemically reacted with tin species to form a surface complex on the cassiterite surface.

3.5. FTIR Analysis

Figure 11 shows the FTIR spectra of SLG, cassiterite, and cassiterite treated with SLG at pH 7.8 ± 0.2. As shown, for SLG, the bands at 3430.5 cm^{-1} and 3271.3 cm^{-1} are related to the stretching vibration of N-H. The peaks at 2918.4 cm^{-1} and 2850.1 cm^{-1} are attributed to the characteristic peak of -CH_2- and CH_3- groups, and the peak at 1641.2 cm^{-1} corresponds to the stretching vibration of the amide carbonyl in -CON-. The peaks at 1547.5 cm^{-1} and 1408.2 cm^{-1} are caused by the bending vibration of N-H and the stretching vibration of C-O. In addition, the peak at 558.4 cm^{-1} is due to the C-N stretching vibration. In the cassiterite IR spectrum, the characteristic bond at 3732.5 cm^{-1} belongs to the typical hydroxylate adsorption peak of the O-H vibration. This peak of O-H reflected the hydroxylation that occurred on the cassiterite surface in the pulp. The characteristic bond at 1620.2 cm^{-1} is attributed to the H_2O adsorption on the surface of the minerals. The peaks at 655.3 cm^{-1} and 582.6 cm^{-1} represent the stretching vibration of the Sn-O vibration.

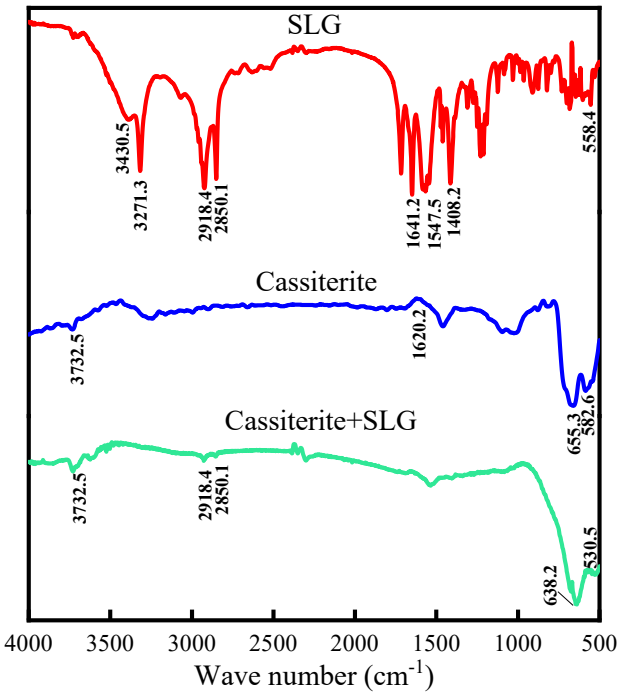

Figure 11. FTIR spectra of SLG, cassiterite, and SLG-treated cassiterite.

After treating cassiterite with SLG, new adsorption peaks appeared in the FTIR spectra of cassiterite at 2918.4 cm^{-1} and 2850.1 cm^{-1} due to the -CH_2- and CH_3- groups of SLG, indicating that SLG was chemically adsorbed on the cassiterite surface. Meanwhile, the disappearance of the O-H stretching peak at 3732 cm^{-1} may have resulted from the change of the hydroxy on the cassiterite surface. Meanwhile, the N-H stretching peak has vanished, corresponding to the peak at 1547.5 cm^{-1}, in the SLG spectrum. In addition, the new Sn-O vibration at 638.2 cm^{-1} may have resulted from the formation of Sn-O between the SLG and the cassiterite.

A potential formation of SLG adsorbed on the cassiterite surface is suggested in Figure 12. the polar groups of SLG anions (-COO- and -CON groups) chelate with the Sn ions on the cassiterite surface to form five-membered rings, thus forming a stable adsorption structure on the cassiterite surface and resulting in the strong collecting performance of SLG.

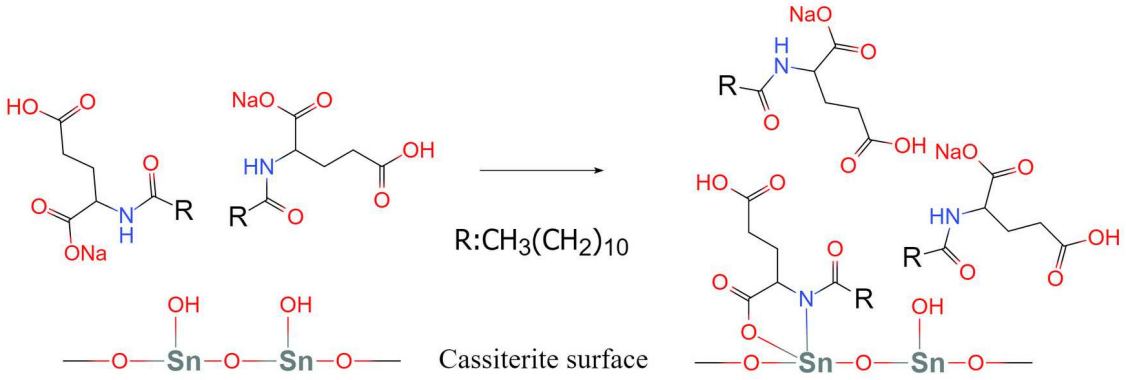

Figure 12. Possible adsorption models of SLG on cassiterite surfaces.

3.6. Bench-Scale Flotation Tests of Xinzhai Cassiterite

The Xinzhai tin deposit belongs to the Laojunshan tin polymetallic metallogenic belt. The main metal minerals are cassiterite, chalcopyrite, sphalerite, marmatite, pyrite, pyrrhotite, and magnetite. Gangue minerals include quartz, feldspar, and epidote. It is difficult to enrich and separate valuable metallic minerals due to their large element content and complex mineral composition. The chemical composition of the mean sample is shown in Table 4, indicating that the average tin grade of the Xinzhai cassiterite was 0.14%.

Table 4. Chemical composition of the Xinzhai cassiterite.

Elements	Sn	Pb	Zn	S	Cu	SiO_2	Fe	Else
Content (wt %)	0.14	0.46	6.89	21.52	0.23	37.5	30.21	3.05

Bench-scale flotation was carried out in an XFD-63 pneumatic flotation machine, using 1.5 L for rougher flotation and 1 L and 0.5 L for cleaner flotation. Before flotation, the raw ore was ground for 8 min in a closed XMQ-240 × 90 ball mill to obtain a sample reaching 71.5% of −74 µm. The raw ore was transferred to the flotation cell with tap water to achieve a pulp density of 30% solids by weight. The slurry was then conditioned for 2 min at 2100 rpm, followed by 3 min of stirring with the required amount of depressant (500 g/t CMC). The suspension was then allowed to condition for 3 min and 2 min with collectors and frothers in sequence. Next, the pulp was floated for 4 min at 1900 rpm with an airflow rate of 7.0 L/min. The rougher stage was followed by two cleaner and two tailing scavenger flotation stages, in which tap water was added to the concentrate of the previous stage to make up the pulp. The simplified flowsheet of the bench-scale flotation tests is shown in Figure 13.

Table 5 lists the flotation indexes produced by adding SLG or BHA. It was observed that grade and recovery in concentrate improved from 3.45% Sn at 74.3% recovery to 4.02% Sn at 85.2% recovery before and after SLG treatment. The SLG collector has achieved a satisfying effect in practical applications.

Table 5. Results of closed-flotation operation for Xinzhai cassiterite (%).

Conditions	Product	Yield	Sn Grade	Sn Recovery
BHA	Concentrate	3.09	3.45	74.3
	Tailings	96.91	0.038	25.7
	Raw ore	100	0.144	100
SLG	Concentrate	3.05	4.02	85.2
	Tailings	96.95	0.022	14.8
	Raw ore	100	0.143	100

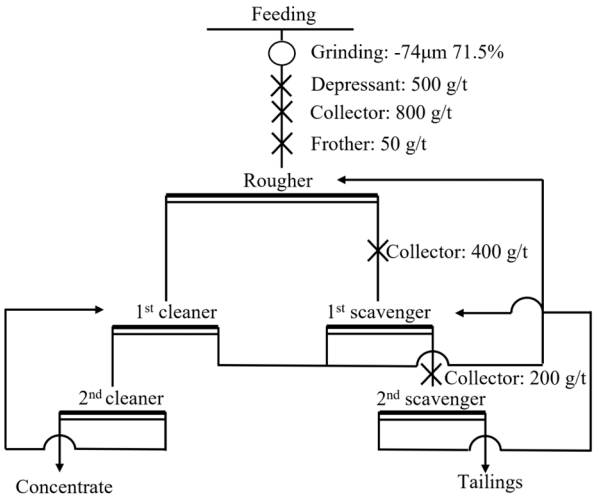

Figure 13. The flowsheet of the bench-scale flotation tests.

4. Conclusions

This paper evaluated and analyzed the flotation performance and adsorption mechanism of SLG on cassiterite by flotation tests, adsorption experiments, zeta potential, XPS, and FTIR analyses. Based on the experimental results, the following conclusions could be drawn:

The micro-flotation results indicated that SLG could effectively collect cassiterite and have superior selectivity against quartz over a wide pH range. Adsorption experiments and zeta potential measurements deduced that SLG might chemisorb on cassiterite surfaces. XPS and FTIR analyses further inferred that the polar groups of SLG anions (the carboxyl and amide groups) chelate with the Sn ions on the cassiterite surface to form five-membered rings. This structure made SLG attach firmly to the cassiterite surface, effectively recovering cassiterite. For Xinzhai tin deposits, grade and recovery in concentrate improved from 3.45% Sn at 74.3% recovery to 4.02% Sn at 85.2% recovery by using SLG as the collector, which confirmed its potential economic value in the practical application of cassiterite.

Author Contributions: Formal analysis, visualization, investigation, writing–original draft, Z.P. and Q.W.; Formal analysis, data curation, investigation, writing–review and editing, L.S.; Investigation, data curation, formal analysis, Y.C.; Methodology, project administration, resources, funding acquisition, supervision, writing–review and editing, X.F.; Conceptualization, methodology, funding acquisition, W.S. All authors have read and agreed to the published version of the manuscript.

Funding: All authors of this work acknowledged the financial support from the National Natural Science Foundation of China (Grant No. 51904338), the Natural Science Foundation of Hunan Province, China (Grant No. 2020JJ5746), the National Key R&D Program, China (Grant No. 2020YFC1909202), and the Collaborative Innovation Center for Clean and Efficient Utilization of Strategic Metal Mineral Resources.

Data Availability Statement: Data that support the findings of this study are available from the corresponding author upon reasonable request.

Acknowledgments: We sincerely thank the Editorial board members and three anonymous reviewers for their constructive comments.

Conflicts of Interest: The authors declare no conflict of interest.

References

1. Cao, Y.; Sun, L.; Gao, Z.; Sun, W.; Cao, X. Activation mechanism of zinc ions in cassiterite flotation with benzohydroxamic acid as a collector. *Miner. Eng.* **2020**, *156*, 106523. [CrossRef]
2. Matveeva, T.N.; Chanturia, V.A.; Gromova, N.K.; Lantsova, L.B. Effect of chemical and phase compositions on absorption and flotation properties of tin–sulphide ore tailings with dibutyl dithiocarbamate. *J. Min. Sci.* **2018**, *54*, 1014–1023. [CrossRef]

3. Yang, C.; Tan, Q.; Zeng, X.; Zhang, Y.; Wang, Z.; Li, J. Measuring the sustainability of tin in China. *Sci. Total Environ.* **2018**, *635*, 1351–1359. [CrossRef] [PubMed]
4. Qi, J.; Liu, S.; Dong, Y.; Liu, G. Revealing the role of dithiocarbamate ester group in hydroxamic acid flotation of cassiterite with in situ AFM, DFT and XPS. *Appl. Surf. Sci.* **2022**, *604*, 154521. [CrossRef]
5. Angadi, S.I.; Sreenivas, T.; Jeon, H.S.; Baek, S.H.; Mishra, B.K. A review of cassiterite beneficiation fundamentals and plant practices. *Miner. Eng.* **2015**, *70*, 178–200. [CrossRef]
6. Sun, L.; Hu, Y.; Sun, W. Effect and mechanism of octanol in cassiterite flotation using benzohydroxamic acid as collector. *Trans. Nonferrous Met. Soc. China* **2016**, *26*, 3253–3257. [CrossRef]
7. Ren, L.; Qiu, H.; Zhang, M.; Feng, K.; Liu, P.; Guo, J.; Feng, J. Behavior of lead ions in cassiterite flotation using octanohydroxamic acid. *Ind. Eng. Chem. Res.* **2017**, *56*, 8723–8728. [CrossRef]
8. Wang, X.; Liu, J.; Zhu, Y.; Li, Y. Adsorption and depression mechanism of an eco-friendly depressant PBTCA on fluorite surface for the efficient separation of cassiterite from fluorite. *Miner. Eng.* **2021**, *171*, 107124. [CrossRef]
9. Richards, R.G.; Machunter, D.M.; Gates, P.J.; Palmer, M.K. Gravity separation of ultra-fine (−0.1 mm) minerals using spiral separators. *Miner. Eng.* **2000**, *13*, 65–77. [CrossRef]
10. Cao, Y.; Tong, X.; Xie, X.; Song, Q.; Zhang, W.; Du, Y.; Zhang, S. Effects of grinding media on the flotation performance of cassiterite. *Miner. Eng.* **2021**, *168*, 106919. [CrossRef]
11. Chen, Y.; Tong, X.; Feng, D.; Xie, X. Effect of Al (III) ions on the separation of cassiterite and clinochlore through reverse flotation. *Minerals* **2018**, *8*, 347. [CrossRef]
12. Li, F.; Zhong, H.; Zhao, G.; Wang, S.; Liu, G. Flotation performances and adsorption mechanism of α-Hydroxyoctyl phosphinic acid to cassiterite. *Appl. Surf. Sci.* **2015**, *353*, 856–864. [CrossRef]
13. Lv, L.; Wang, X.; Ren, H.; Liu, J.; Zhu, Y. Depressing Behaviors and Mechanism of an Eco-Friendly Depressant on Flotation Separation of Cassiterite and Fluorite. *J. Mol. Liq.* **2021**, *322*, 114898. [CrossRef]
14. Wang, X.; Miles, N.J.; Kingman, S. Numerical study of centrifugal fluidized bed separation. *Miner. Eng.* **2006**, *19*, 1109–1114. [CrossRef]
15. Bru, K.; Sousa, R.; Leite, M.M.; Broadbent, C.; Stuart, G.; Pashkevich, D.; Martin, M.; Kern, M.; Parvaz, D.B. Pilot-Scale Investigation of two electric pulse fragmentation (EPF) approaches for the mineral processing of a low-grade cassiterite schist ore. *Miner. Eng.* **2020**, *150*, 106270. [CrossRef]
16. Leistner, T.; Embrechts, M.; Leißner, T.; Chehreh Chelgani, S.; Osbahr, I.; Möckel, R.; Peuker, U.A.; Rudolph, M. A study of the reprocessing of fine and ultrafine cassiterite from gravity tailing residues by using various flotation techniques. *Miner. Eng.* **2016**, *96*, 94–98. [CrossRef]
17. Zhou, Y.; Tong, X.; Song, S.; Wang, X.; Deng, Z.; Xie, X. Beneficiation of cassiterite fines from a tin tailing slime by froth flotation. *Sep. Sci. Technol.* **2014**, *49*, 458–463. [CrossRef]
18. Yuan, Q.; Mei, G.; Liu, C.; Cheng, Q.; Yang, S. A novel sulfur-containing ionic liquid collector for the reverse flotation sepa-ration of pyrrhotite from magnetite. *Sep. Purif. Technol.* **2022**, *303*, 122189. [CrossRef]
19. Chen, Y.; Li, H.; Feng, D.; Tong, X.; Hu, S.; Yang, F.; Wang, G. A recipe of surfactant for the flotation of fine cassiterite particles. *Miner. Eng.* **2021**, *160*, 106658. [CrossRef]
20. Jin, S.; Zhang, P.; Ou, L.; Zhang, Y.; Chen, J. Flotation of cassiterite using alkyl hydroxamates with different Carbon Chain Lengths: A Theoretical and Experimental Study. *Miner. Eng.* **2021**, *170*, 107025. [CrossRef]
21. Gong, G.; Wang, P.; Liu, J.; Han, Y.; Zhu, Y. Effect and mechanism of Cu(II) on flotation separation of cassiterite from fluorite. *Sep. Purif. Technol.* **2020**, *238*, 116401. [CrossRef]
22. Tian, M.; Zhang, C.; Han, H.; Liu, R.; Gao, Z.; Chen, P.; He, J.; Hu, Y.; Sun, W.; Yuan, D. Novel insights into adsorption mechanism of benzohydroxamic acid on lead (II)-activated cassiterite surface: An integrated experimental and computational study. *Miner. Eng.* **2018**, *122*, 327–328. [CrossRef]
23. Feng, Q.; Zhao, W.; Wen, S.; Cao, Q. Activation mechanism of lead ions in cassiterite flotation with salicylhydroxamic acid as collector. *Sep. Purif. Technol.* **2017**, *178*, 193–199. [CrossRef]
24. Sreenivas, T.; Padmanabhan, N.P.H. Surface chemistry and flotation of cassiterite with alkyl hydroxamates. *Colloids Surf. A.* **2002**, *205*, 47–59. [CrossRef]
25. Wu, X.; Zhu, J. Selective flotation of cassiterite with benzohydroxamic acid. *Miner. Eng.* **2006**, *19*, 1410–1417. [CrossRef]
26. Zhao, G.; Wang, S.; Zhong, H. Study on the activation of scheelite and wolframite by lead nitrate. *Minerals* **2015**, *5*, 247–258. [CrossRef]
27. Tian, M.; Gao, Z.; Han, H.; Sun, W.; Hu, Y. Improved flotation separation of cassiterite from calcite using a mixture of lead (II) ion/benzohydroxamic acid as collector and carboxymethyl cellulose as depressant. *Miner. Eng.* **2017**, *113*, 68–70. [CrossRef]
28. Shukla, V.; Shukla, P.; Tiwari, A. Lead Poisoning. Lead poisoning. *Indian J. Med. Spec.* **2018**, *9*, 146–149. [CrossRef]
29. Izard, C.F.; Müller, D.B. Tracking the devil's metal: Historical global and contemporary U.S. tin cycles. *Resour. Conserv. Recycl.* **2010**, *54*, 1436–1441. [CrossRef]
30. Marques, E.F.; Brito, R.O.; Silva, S.G.; Enrique Rodríguez-Borges, J.; do Vale, M.L.; Gomes, P.; Araújo, M.J.; Söderman, O. Spontaneous vesicle formation in catanionic mixtures of amino acid-based surfactants: Chain length symmetry effects. *Langmuir* **2008**, *24*, 11009–11017. [CrossRef]

31. Islam, M.S.; Shortall, S.M.; Mekhail, G.M.; Callender, S.P.; Madkhali, O.; Bharwani, Z.; Ayyash, D.; Kobernyk, K.; Wettig, S.D. Effect of counterions on the micellization and monolayer behaviour of cationic gemini surfactants. *Phys. Chem. Chem. Phys.* **2017**, *19*, 10825–10834. [CrossRef]
32. Ariki, R.; Hirano, A.; Arakawa, T.; Shiraki, K. Drug solubilization effect of Lauroyl-L-glutamate. *J. Biochem.* **2012**, *151*, 27–33. [CrossRef] [PubMed]
33. Ananthapadmanabhan, K.P. Amino-Acid Surfactants in Personal Cleansing (Review). *Tenside Surfactants Deterg.* **2019**, *56*, 378–386. [CrossRef]
34. Bordes, R.; Holmberg, K.A. Amino acid-based surfactants—Do they deserve more attention? *Adv. Colloid Interface Sci.* **2015**, *222*, 79–91. [CrossRef]
35. Katiyar, S.S.; Kushwah, V.; Dora, C.P.; Patil, R.Y.; Jain, S. Design and toxicity evaluation of novel fatty acid-amino acid-based biocompatible surfactants. *AAPS PharmSciTech* **2019**, *20*, 186. [CrossRef]
36. Sivasamy, A.; Krishnaveni, M.; Rao, P.G. Preparation, characterization, and surface and biological properties of N-stearoyl amino acids. *J. Am. Oil Chem. Soc.* **2001**, *78*, 897–902. [CrossRef]
37. Zhou, C.; Liu, L.; Chen, J.; Min, F.; Lu, F. Study on the influence of particle size on the flotation separation of kaolinite and quartz. *Powder Technol.* **2022**, *408*, 897–902. [CrossRef]